

RESEARCH ARTICLE

First-story height effects on the collapse performance of buildings in extreme events

Necmettin Güneş^{1*}, Pınar Bora²

- ¹ Sivas Cumhuriyet University, Department of Architecture, Sivas, Türkiye
- ² Sivas Cumhuriyet University, Department of Civil Engineering, Sivas, Türkiye

Article History

Received 29 May 2024 Accepted 1 July 2024

Keywords

First-story height Vertical irregularity Ductility capacity Incremental dynamic analysis Collapse probability

Abstract

Higher first-story height could cause soft-story irregularity due to less lateral stiffness, in which the hysteric energy dissipation is localized at the first story of buildings. In the seismic design codes, two different approaches, based on the drift and lateral stiffness ratios, are used to determine soft-story irregularity. In this study, four reinforced concrete models with different first-story to typical-story height ratios are used to show the first-story height effects. It is shown that even if the models are regular for soft stories based on the seismic design code limits, the higher first story considerably decreases the ductility capacity. Also, it is demonstrated that the ductility capacity is highly correlated with the story height ratio. Although all models meet the design criteria of the Turkish Buildings and Earthquake Code (TBEC-2018), the results of the nonlinear time history analysis reveal that the first-story drift ratio considerably increases with the higher first-story height. Further, the collapse performance of the four models is determined using the FEMA P695 procedure, and the results demonstrate that the collapse probability of the model with the highest first-story height is over the ASCE 7-22 limit.

1. Introduction

Since the ground stories of the buildings on the street are generally used for commercial purposes, their story heights are higher than the upper stories' height. This problem might cause soft-story irregularity. Seismic design codes determine soft-story irregularity based on the lateral stiffness and story drift ratio parameters. According to ASCE 7-22 [1], the soft-story irregularity is defined as the lateral stiffness of any story below 70% of that of the above story. Also, when the lateral stiffness of any story is below 80% of the average stiffness of three upper stories, it is defined as a soft-story irregularity. However, these two criteria are valid when the story drift ratio exceeds 130% of an adjacent story drift ratio. In the TBEC-2018 [2], soft story irregularity is defined as the drift ratio of any story being more than twice that of the upper or lower story drift ratios.

In the literature, many studies demonstrate the effects of soft-story irregularity on the performance of buildings [3–6]. Scarlat [7] proposed an energy-based method to design the structural members of soft stories.

eISSN 2630-5763 © 2023 Authors. Publishing services by golden light publishing®.

^{*} Corresponding author (ngunes@cumhuriyet.edu.tr)

İnel and Meral [8] showed that the soft-story irregularity considerably causes a decrease in the lateral load capacity and roof drift ratio for substandard buildings.

ASCE 7-22 [1] and TBEC-2018 [2] require using the mode-combination method instead of the equivalent lateral load method for buildings with soft-story irregularity. Also, ASCE 7-22 prohibits using buildings with extreme soft story irregularity, in which the stiffness ratio of any story to that of the above story is lower than 60%, in the higher seismic risk design categories, such as E and F. However, NTCS-2004 [9] proposes to decrease the response modification factor for irregular buildings and to overcome the effects of soft-story irregularity on the buildings, the lateral design load of buildings with soft-story irregularity is taken higher than that of the regular buildings [4,9–11].

All the above studies focus on buildings with soft-story irregularity. However, in some buildings, the first or ground story is higher than the upper stories, but the height differences do not cause the soft-story irregularity according to the seismic design code limits. Since these types of buildings are common in Türkiye, it is essential to figure out the collapse performance of such buildings in extreme events. Also, it is needed to show the validation of the using the same response modification factor for such buildings.

In this study, four Reinforced Concrete (RC) models with different first-story heights were designed, and the story drift ratios were obtained at the design phase following TBEC-2018. Then, the response modification factors were obtained using pushover analyses, and the results demonstrated that the acquired response modification factor might differ according to the height ratio of the first story to the typical story. Further, it was shown that the elastic analysis might not capture the soft-story mechanism-like behavior of such buildings. After that, the collapse probabilities were obtained using FEMA P695 [12] at the DD-1 earthquake level, whose return period is 2475 years according to the TBEC-2018.

2. Model descriptions

The typical plan and elevation views of the used 5-story RC building models are given in Fig. 1. The typical story height is 3.1 m, and the first-story heights of the four models are 3.1 m, 3.5 m, 3.9 m, and 4.3 m, respectively. It was assumed that the models were located at 41.048937° (latitude), and 29.068002° (longitude) coordinates, and the soil type was ZC according to the TBEC-2018. Also, the short-period geometric mean spectral acceleration values (SDS) were taken as 0.959g and 1.690g for DD-2 and DD-1 earthquake levels from the Turkish Seismic Hazard Map (TSHM) [13]. The long-period geometric mean spectral acceleration values (SD1) were 0.337g and 0.586g for DD-2 and DD-1 earthquake levels according to the TSHM [13].

2.1. Design of models

The superimposed dead and live loads were 1.5 kN/m^2 , 2.0 kN/m^2 . The partition walls were considered for all stories except the roof story, and their weights for the outer and inner beams were 9.88 kN/m and 6.5 kN/m, respectively. The specified concrete and reinforcement rebar strengths were 30 MPa and 420 MPa. The elastic analysis and design of models were carried out using Etabs [14] software, and the effective flexural stiffnesses of columns and beams were modified using 0.7 and 0.35 factors, respectively, as recommended in TBEC-2018. The mode superposition method was used for elastic design. For all models, the slab thickness was 0.18 m, and the dimensions and longitudinal (ρ_1) and transverse (ρ_t) reinforcement ratio ranges are given in Table 1 for columns and beams. All models fulfilled the strong column-weak beam criteria of the TBEC-2018. Also, for all load combinations with seismic load, the axial loads of all columns were below the $0.4f_{ck}A_c$ value, where the f_{ck} and A_c were the specified concrete strength and the cross-section area.

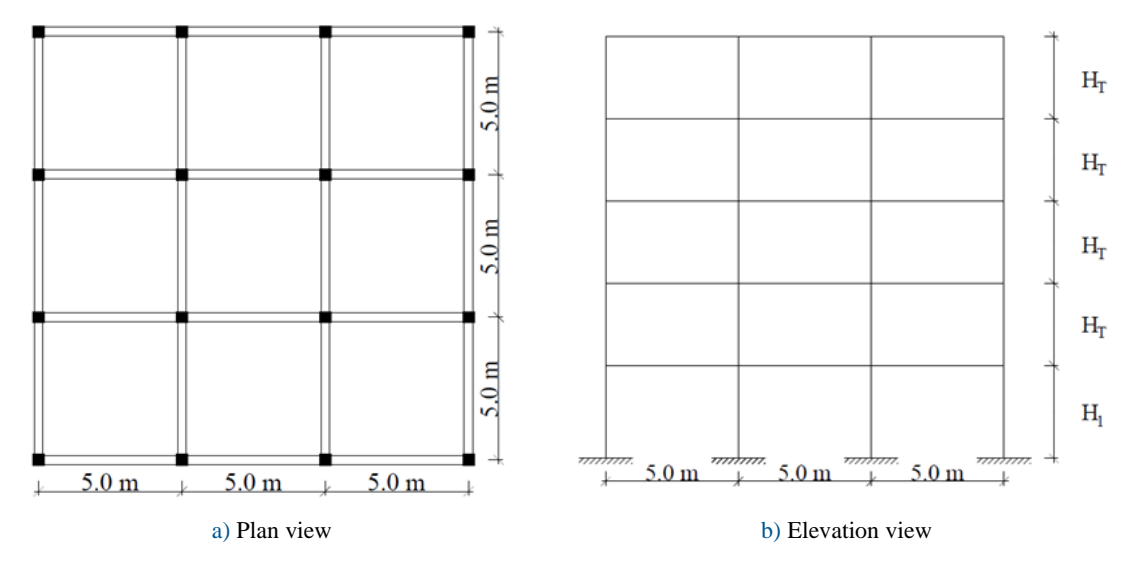


Fig. 1. View of typical a) plan b) elevation

2.2. Nonlinear modeling

The stress-strain curves for the concrete and reinforcement rebar were acquired using the Mander concrete model [15] and the TBEC-2018, respectively. The nonlinear behavior of beams was modeled using the concentrated plastic hinges at both ends. Also, the cyclic degradation effect was considered as recommended in PEER-ATC [16] and Haselton et al. [17] studies. As given in Fig. 2, the nonlinear modeling of columns was represented by the fiber hinge elements at both ends, and the part between these hinge members was elastically modeled with the effective stiffness, as recommended by Berry and Eberhard [18] and NIST [19]. Also, the fiber hinge length (L_p) was obtained using Berry and Eberhard's study [18].

Table 1. Dimensions and reinforcement details for columns and beams

Member	Dimension (cm/cm)	ρι (max)/ρι (min) (%)	p _t (%)	ρ _l (max)/ρ _l (min) (%) (top)	$\rho_l \text{ (max)/}\rho_l \text{ (min)}$ (%) (bottom)
Column	45x45	1.27/1.27	0.45	-	-
Beam	30x50	-	0.4	0.71/0.41	0.41/0.41

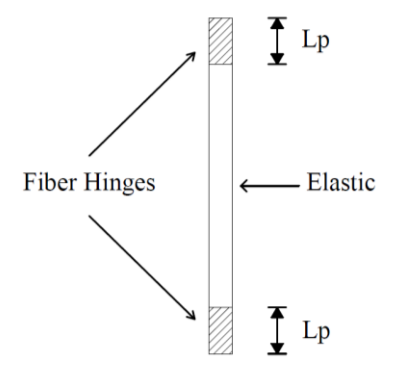


Fig. 2. Column nonlinear modeling (adopted from NIST [19])

3. Degrees of vertical irregularity

In the seismic design codes [1,2], soft-story irregularity is defined by story stiffness or story drift ratios. Since the first or ground story was higher than the other, the story drift ratios obtained in the design phase and story stiffnesses were normalized with the first-story values (Fig. 3) to enable a comparison. The TBEC-2018 gives the lower limit ratio of two adjacent story drift ratios for soft story irregularity as 2. In Fig. 3a, all normalized drift ratios were below 2. Therefore, all models had no soft-story irregularity for this seismic code. In Fig. 3b, all values were below 1.43 (1/0.7), which corresponds to the second-story stiffness to the first-story stiffness ratios for the ASCE 7-22 limit. Notwithstanding the ratio of the average story stiffness of three stories above the first-story to the first-story stiffness was 0.793, the ratio of the first-story drift ratio to the second-story drift ratio was below 1.3 for the fourth model, in which the first-story height was 4.3 m. Therefore, all models had no soft-story irregularity according to ASCE 7-22.

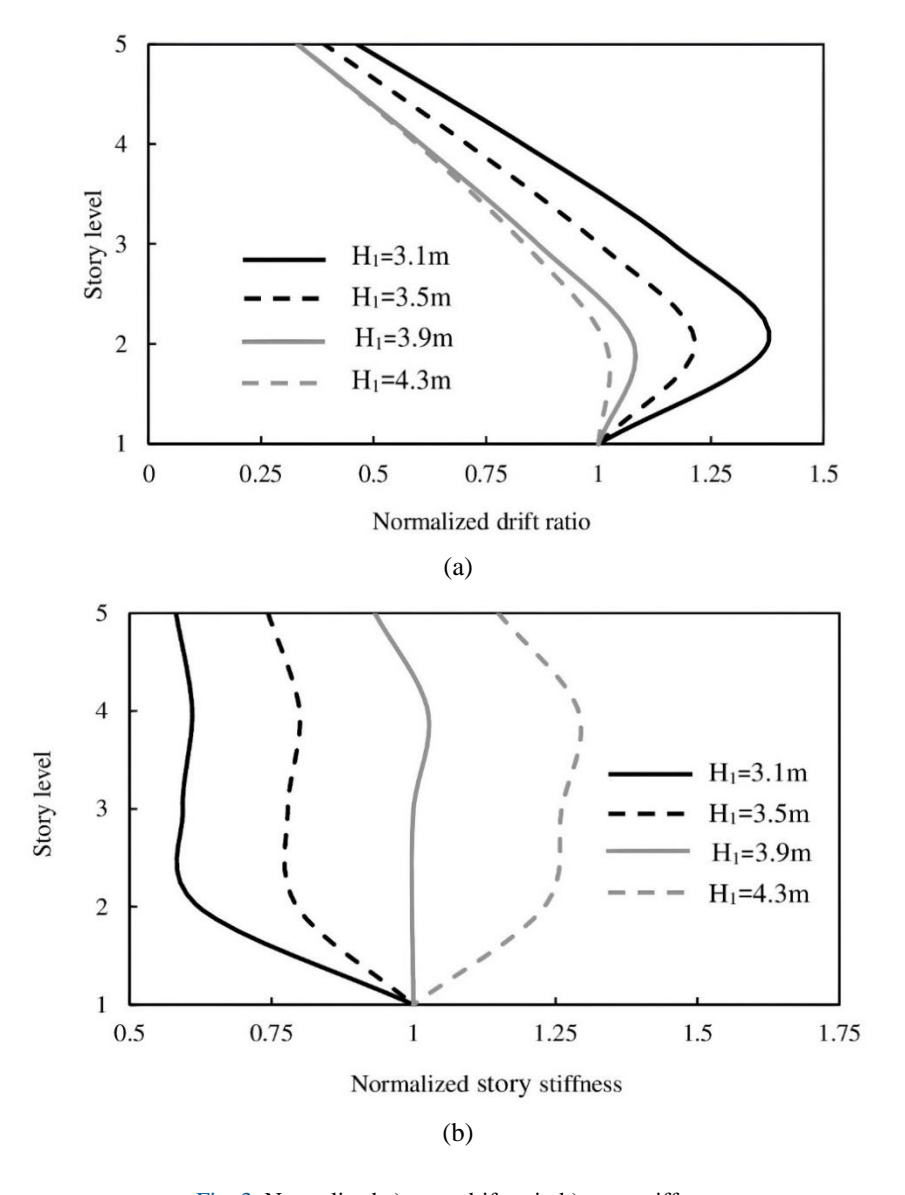


Fig. 3. Normalized a) story drift ratio b) story stiffness

4. Nonlinear static and nonlinear time history analyses

4.1. Nonlinear static analyses

Nonlinear static (pushover) analysis has been utilized for RC and masonry buildings to determine seismic performance and yielding mechanics [20–22]. Also, seismic design codes [1,2] recommend using the overstrength factor (Ω), the ratio of lateral load capacity to design base shear, to validate design requirements using pushover curves.

FEMA P695 [12] proposes a procedure to idealize pushover curves. In Fig. 4, these idealized curves were given for four models. In these curves, firstly, the lateral load capacity of the pushover curve (V_{max}) was determined then the effective yielding displacement ($\delta_{y,eff}$) was obtained using the tangent line to the initial part of the pushover curve. After that, the ultimate or near-collapse displacement (δ_u), where the base shear equals 80% of the V_{max} value in the decreasing part of pushover curves, was obtained. Then the period-based ductility (μ_T), also known as near-collapse ductility [23], was acquired as the ratio of the δ_u to $\delta_{v,eff}$.

TBEC-2018 limits the lower bound of the overstrength factor with 3 for the ductile design of the RC framed buildings. In Table 2, overstrength and ultimate ductility factors for used models were given. Although the overstrength factors were over the TBEC-2018 lower limit, the ultimate ductility considerably decreased when the first-story height was increased. This situation meant that the higher first-story height caused a considerable decrease in the energy dissipation capacity of buildings. When it was assumed that the response modification factor was equal to the ductility in the period range of velocity- and -displacement sensitive regions, as given TBEC-2018, the relation between the response modification factor and the ratio of first-story height (H₁) to the typical story height (H_T) was shown in Fig. 5.

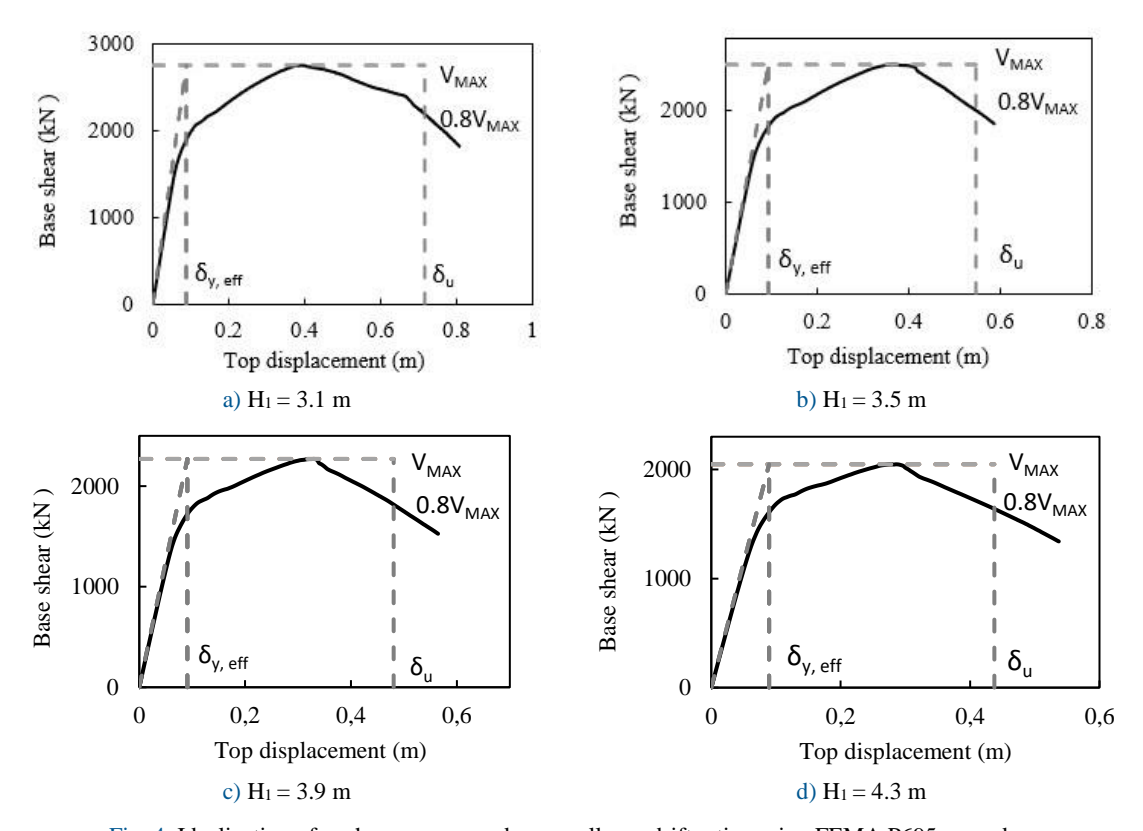


Fig. 4. Idealization of pushover curve and near-collapse drift ratios using FEMA P695 procedure

Model	Ω	μ_{T}				
1	4.9	8.0				
2	4.7	5.8				
3	4.5	5.3				
4	4.1	4.9				

Table 2. Overstrength and ultimate ductility factors using FEMA P695 procedure

NTCS-04 [9] and the Manual of Civil Structures (MOC) [24] increase the design force by limiting the reduction of elastic force for irregular buildings. In the MOC [24], the reductive seismic force factor is taken as 80% of that of regular buildings to increase the lateral design force for buildings with soft-story irregularity [11]. This requirement meant that the response modification factor was decreased by 20% to increase the design base shear. Since the increasing design force could prevent or limit the soft-story mechanics, the nonlinear behavior might be distributed toward the upper stories. Therefore, the increasing ductility probably was higher than the decreasing response modification factor. For this reason, the response modification factor given in Fig. 5 was likely conservative for models 2 to 4. However, the MOC limit is shown in Fig. 5 to illustrate the effect of the localization of nonlinear behavior in the first story on the energy dissipation capacity of models.

4.2. Nonlinear time history analyses

The energy dissipation capacity decreased considerably due to higher first-story height, as shown in Fig. 4. Therefore, it was essential to demonstrate the distribution of nonlinear behavior along the height of buildings. For this reason, all models were subjected to the FEMA P695 far-field records in one direction, and all these records were downloaded from the PEER ground motion database [25]. TBEC-2018 requires amplitude scaling of records in the period range of $0.2T_p$ and $1.5T_p$, where the T_p is the first mode period. All ground motions were scaled to the DD-1 level maximum-direction spectrum following TBEC-2018. Since the periods of nonlinear models were different, the scaling procedure was separately employed for all models, and the target maximum direction and the mean scaled spectra are given in Fig. 6 for Model 1.

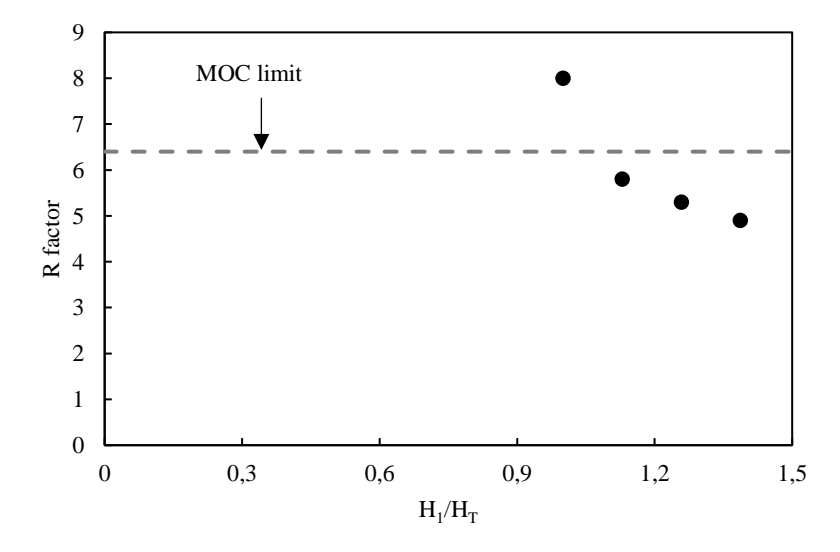


Fig. 5. The relation between the H₁/H_T ratios and R factors

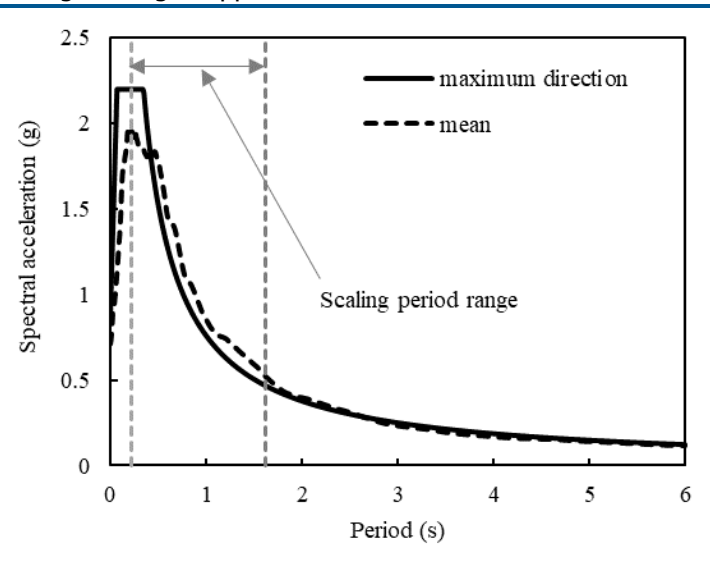


Fig. 6. DD-1 level maximum direction and mean scaled spectra for Model 1

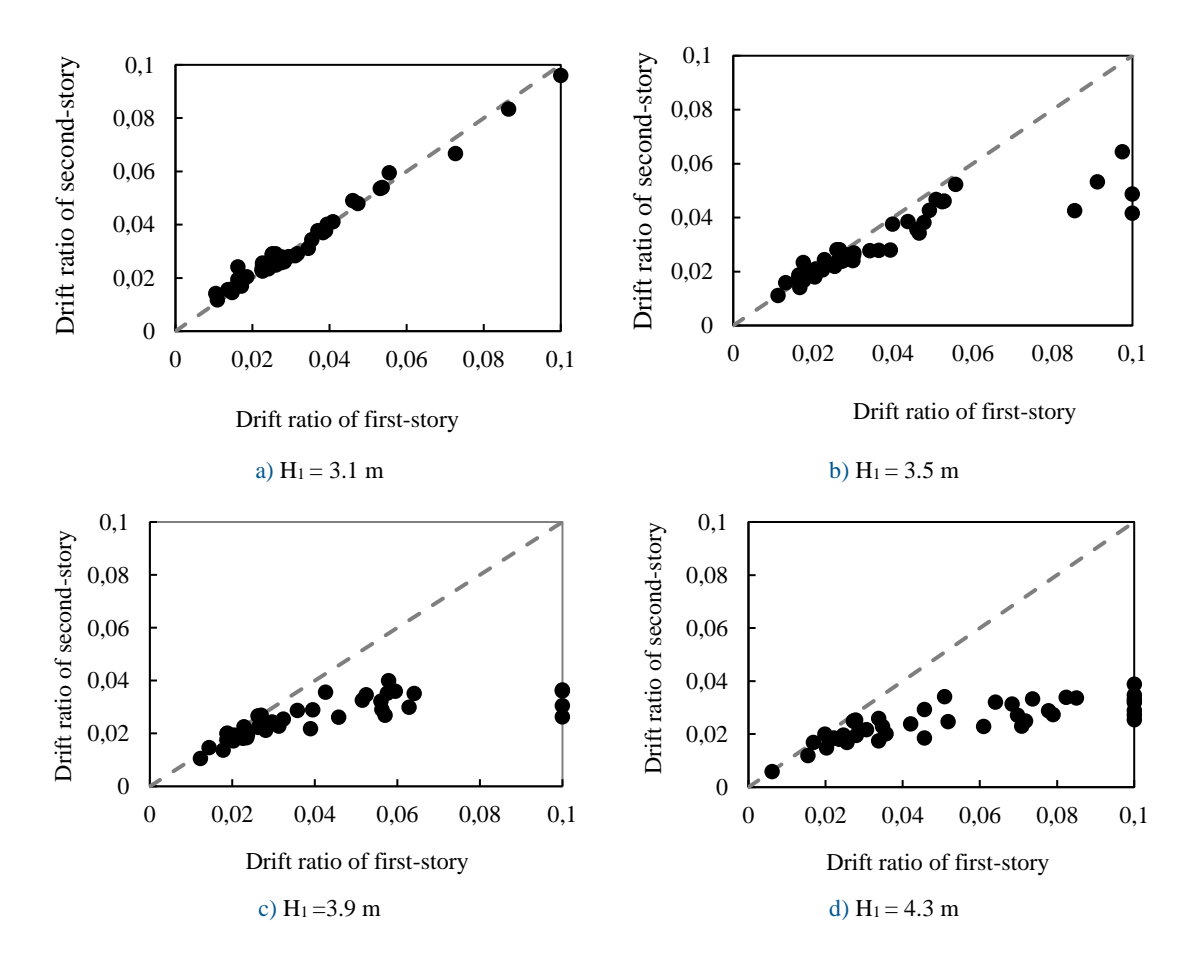


Fig. 7. Relation between the drift ratio of first and second stories

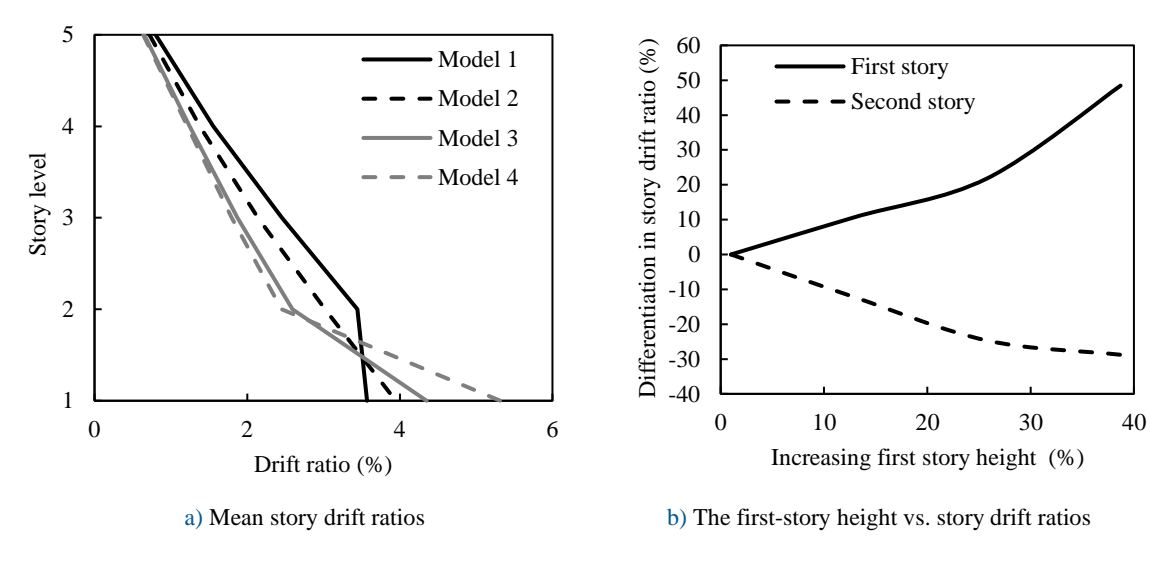


Fig. 8. NTH analysis results for a) mean story drift ratios b) relation between the first-story height and story drift ratios

In Fig. 7, the relations between the first- and second-story drift ratios were given for the four models using 44 NTH analysis results, and it was assumed that the models arrived at collapse capacity when the drift ratio of any story reached a 10% value. When the first- and upper-story heights were equal, the second-story drift ratios were very close to the first-story ones, as shown in Fig. 7a. This phenomenon meant that the nonlinear behavior was not localized in the first-story but distributed in the upper stories. However, when the first-story height was higher than that of the upper stories, the linear relation between the drift ratios of the first and second stories was disturbed (Fig. 7b-d). Further, the drift ratios of the second-story decreased by increasing the first-story height.

The mean story drift ratios were given in Fig. 8a to summarize the above phenomenon. The first- and second-story drift ratios for Model 1 were 3.57% and 3.44%. However, when the first-story height was increased from 3.1 m to 4.3 m, the first-story drift ratio increased to 5.3%, and the second-story drift ratio decreased to 2.45%. Thus, the percent increases in first-story height and first-story drift ratio were 38.7% and 48.5%, respectively. Meanwhile, the percent decrease in the second-story drift ratio was 28.8%. Other values are given in Fig. 8b.

In the literature [26], the soft-story mechanism is given in detail. Although no one model had soft-story irregularity according to the seismic codes [1,2] limits, the nonlinear behavior concentrated at the first-story level by increasing the first-story height. This phenomenon was similar to the soft-story mechanism. However, seismic design codes required the using the mode-superposition method, and it was not possible to capture the soft-story mechanism-like behavior using elastic methods.

5. Incremental dynamic analysis

Incremental dynamic analysis (IDA) has been used to obtain the fragility curve [27]. In IDA, a record set is used and the analytical structure model is subjected to each of the scaled records, and the scaling factor is increased up to the collapse point. Thus, the relation between the desired Intensity Measure (IM) parameter and the Engineering Demand Parameter (EDP) is obtained using these NTH analysis results. The spectral acceleration of the first mode period (Sa(T1)) and inter-story drift ratio (IDR) have been utilized as IM and IDR in the literature [27,28].

The lognormal cumulative distribution function has been used to obtain fragility curves [29–31], which is given in Equation 1.

$$P\{C|IM = x\} = \Phi\left(\frac{\ln\left(\frac{x}{\theta}\right)}{\beta}\right) \tag{1}$$

In Eq. 1, Φ is the standard normal cumulative distribution function, θ is the median value of the probability distribution, and β is the logarithmic standard deviation. These parameters were estimated using the method proposed by Baker's [31] study.

FEMA P695 proposes a procedure to consider the spectral shape effect and various uncertainties. The spectral shape effect stems from using the same record set for all the IM levels [32–34], and the FEMA P695 procedure uses the specified Spectral Shape Factor (SSF) to modify the fragility function to eliminate the spectral shape effects of IDA analysis. Also, FEMA P695 requires considering the four uncertainty parameters to obtain total uncertainty (β_{TOT}) as given in Eq. 2.

$$\beta_{TOT} = \sqrt{\beta_{RTR}^2 + \beta_{DR}^2 + \beta_{TD}^2 + \beta_{MDL}^2}$$
 (2)

where the β_{RTR} , β_{DR} , β_{TD} , and β_{MDL} are the record-to-record variation, design requirement, test data, and modeling uncertainty parameters, respectively.

The β_{RTR} parameter was taken as the logarithmic deviation of the fitted fragility curve, and the quality ratings for the β_{DR} , β_{TD} , and β_{MDL} parameters were taken as 0.2, which refers to a good quality rate according to the FEMA P695. Also, the SSF factors were obtained utilizing period-based ductilities and fundamental mode period following FEMA P695. For all models, the SSF factors and β_{TOT} parameters are given in Table 3.

The exceedance probabilities of the near-collapse drift ratio were obtained using fragility curves. In Fig. 9a, the fitted curves were given for all models. Also, to demonstrate the exceedance probability at the one value, the spectral acceleration axis was normalized with the maximum direction spectral acceleration of the fundamental mode periods $(S_M(T_1))$. The spectral shape factors and total uncertainty parameters were incorporated into the fitted curves following the FEMA P695 procedure, and the results are given in Fig. 9b.

The exceedance probabilities of near-collapse drift ratios were 2.3% and 5.3% for Models 1 and 2 at the maximum direction of the DD-1 earthquake level. ASCE 7-22 categorizes buildings according to their risk level to human life in four groups, and the permitted collapse probabilities are given as %10 for buildings in the Risk Category of I and II. Also, the upper collapse probability limits for buildings in Risk Categories III and IV are 5% and 2.5%, respectively. Since the exceedance probability of the near-collapse drift ratio represented the collapse probability, the obtained collapse probabilities for Models 1 and 2 were below the ASCE 7-22 limit, which is 10% for the buildings in Risk Category I and II. For Model 3, the collapse probability was 9.1%, and it was close to the ASCE 7-22 limit. For Model 4, the collapse probability was %13.1, and it was over the ASCE 7-22 limit.

Table 3. Spectral shape factors (SSF) and total uncertainties (β_{TOT}) (obtained from FEMA P695).

Model SSF

Model	SSF	$eta_{ ext{TOT}}$
1	1.463	0.610
2	1.407	0.629
3	1.40	0.617
4	1.393	0.609

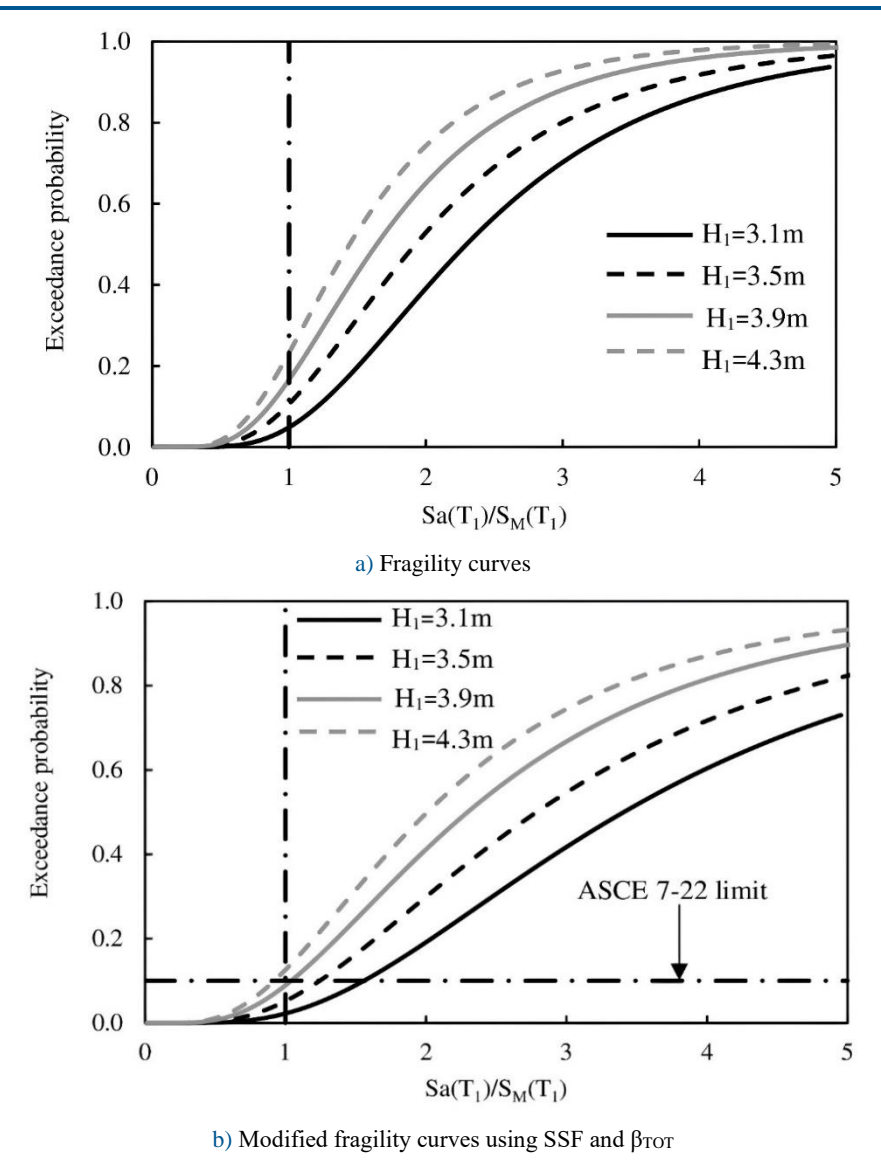


Fig. 9. Fragility curves for models

6. Conclusions

The first-story height is higher than the typical story height when the first or ground story is used for commercial purposes, and this case might cause soft-story irregularity. In the seismic design codes, the soft-story irregularity is defined using inter-story drift and story stiffness ratios. Although the first-story height is higher than the typical story height for some buildings, they are not categorized as soft-story buildings when the inter-story drift ratios and stiffness ratios of two adjacent stories fulfill the seismic design codes' regular building limits.

In this study, four models with different first-story height to typical story height ratios but vertically regular according to the TBEC-2018 and ASCE 7-22 criteria were analyzed at the maximum direction of DD-1 earthquake level, and collapse performances were obtained following the FEMA P695 procedure. The obtained results were given as follows:

- 1. The ductility capacity of the buildings decreased with the increasing H₁/H_T ratio, and this finding was consistent with the previous studies.
- 2. With the increase in the H₁/H_T ratio, the structural damage in the first-story considerably increased. Since the localization of the damage in the first story, the inter-story drift ratios of the upper story decreased. Further, it was not possible to capture this issue using elastic analysis methods such as equivalent load and mode superposition methods.
- 3. The exceedance probability of the near-collapse drift ratio increased with the increase of the H_1/H_T ratio. Also, for the model with the H_1/H_T ratio of 1.3, the exceedance probability of the near-collapse drift ratio was 13%, and it was over the ASCE 7-22 limit.
- 4. For all models, the drift ratio of the second-story was higher than that of the first-story using the mode superposition method. However, the results of the NTH analyses at the maximum direction of the DD-1 earthquake level showed that the first-story drift ratio was higher than that of the upper stories for all models.
- 5. It was recommended to use the pushover analysis to see the global ductility capacity when the first story was higher than the upper stories.

Declaration of conflicting interests

The author(s) declared no potential conflicts of interest with respect to the research, authorship, and/or publication of this article.

Funding

This research received no external funding.

Data availability statement

Data generated during the current study are available from the corresponding author upon reasonable request.

References

- [1] ASCE (2022) Minimum Design Loads and Associated Criteria for Buildings and Other Structures (ASCE/SEI 7-22). American Society of Civil Engineers, Structural Engineering Institute, Reston, Virginia.
- [2] TBEC-2018 (2018) Turkish Building Earthquake Code. Disaster and Emergency Management Presidency.
- [3] Sucuoğlu H, Yazgan U, Yakut A. (2007) A screening procedure for seismic risk assessment in urban building stocks. Earthq. Spectra 23:441–458. https://doi.org/10.1193/1.2720931.
- [4] Tena-Colunga A, Hernández-García DA (2020) Peak seismic demands on soft and weak stories models designed for required code nominal strength. Soil Dyn. Earth. Eng. 129. https://doi.org/10.1016/j.soildyn.2019.05.037.
- [5] Inel M, Ozmen HB, Bilgin H (2008) Re-evaluation of building damage during recent earthquakes in Turkey. Eng. Struct. 30:412–427. https://doi.org/10.1016/j.engstruct.2007.04.012.
- [6] Ulutaş H (2024) Investigation of the Causes of Soft-Story and Weak-Story Formations in Low- and Mid-Rise RC Buildings in Türkiye. Buildings 14:1308. https://doi.org/10.3390/buildings14051308.
- [7] Scarlat AS (1997) Design of soft stories A simplified energy approach. Earthq. Spectra 13:305–315. https://doi.org/10.1193/1.1585947.
- [8] Inel M, Meral E (2016) Seismic performance of RC buildings subjected to past earthquakes in Turkey. Earth. Struct. 11:483–503. https://doi.org/10.12989/eas.2016.11.3.483.
- [9] NTCS-04 (2004) Normas Técnicas Complementarias Para Diseño Por Sismo, Reglamento De Construcciones Para El Distrito Federal. Gaceta Oficial Del Distrito Federal (in Italian).
- [10] Tena-Colunga A (2014) Review of the soft first story irregularity condition of buildings for seismic design. The Open Civil Engineering Journal 4. https://doi.org/10.2174/18741495010040100001.

[11] Tena-Colunga A, Mena-Hernandez U, Pérez-Rocha LE, Avilés J, Ordaz M, Vilar JI (2009) Updated seismic design guidelines for model building code of Mexico. Earthq. Spectra 25:869–898. https://doi.org/10.1193/1.3240413.

- [12] FEMA (2009) Quantification of Building Seismic Performance Factors. Report FEMA P695. Washington, DC.
- [13] TSHM (2018) Turkish Seismic Hazard Map. Disaster and Emergency Management Authority. https://tdth.afad.gov.tr/TDTH/main.xhtml.
- [14] ETABS Version 16.0.2016 (2016) Extended 3D Analysis of Building Systems. Computers and Structures, Inc., NY.
- [15] Mander JB, Priestley MJN, Park R (1989) Theoretical Stress-Strain Model for Confined Concrete. J Struct Eng 114:1804–26.
- [16] PEER (2010) Modeling and Acceptance Criteria for Seismic Design and Analysis of Tall Buildings (PEER/ATC-72-1). Pacific Earthquake Engineering Research Center, Berkeley, CA.
- [17] Haselton CB, Liel AB, Taylor-Lange SC, Deierlein GG (2016) Calibration of model to simulate response of reinforced concrete beam-columns to collapse. ACI Structural Journal 113:1141–52. https://doi.org/10.14359/51689245.
- [18] Berry MP, Eberhard MO (2008) Performance Modeling Strategies for Modern Reinforced Concrete Bridge Columns Performance Modeling Strategies for Modern Reinforced Concrete Bridge Columns. PEER Report 2007/07. Pacific Earthquake Engineering Research Center, Berkeley, CA.
- [19] National Institute of Standards and Technology (NIST) (2010) Nonlinear structural analysis for seismic design. Report NIST GCR 10-917-5. Gaithersburg, Maryland.
- [20] Sucuoğlu H, Günay MS (2011) Generalized force vectors for multi-mode pushover analysis. Earthq. Eng. Struct. Dyn. 40:55–74. https://doi.org/10.1002/eqe.1020.
- [21] Akköse M, Sunca F, Türkay A (2018) Pushover analysis of prefabricated structures with various partially fixity rates. Earthquakes and Structures 14:21–32. https://doi.org/10.12989/eas.2018.14.1.021.
- [22] Isık E, Kutanis M, Engin İ (2016) Displacement of the buildings according to site-specific earthquake spectra. Periodica Polytechnica Civil Engineering 60:37–43. https://doi.org/10.3311/PPci.7661.
- [23] Rejec K, Fajfar P (2014) On the relation between the near collapse limit states at the element and structure level. In: Proceedings of Secod European Conference on Earthquake Engineering and Seismology, Istanbul.
- [24] MOC-2008 (2008) Manual de Diseño de Obras Civiles. Diseño por Sismo. Recomendaciones y Comentarios, Instituto de Investigaciones Eléctricas. Comisión Federal de Electricidad, December (in Spanish).
- [25] PEER (2014) PEER Ground Motion Database. Pacific Earthquake Engineering Research Center, Berkeley, CA.
- [26] Sucuoğlu H, Akkar S (2013) Basic Earthquake Engineering: From Seismology to Analysis and Design. Springer Cham. https://doi.org/10.1007/978-3-319-01026-7.
- [27] Vamvatsikos D, Cornell CA (2002) Incremental dynamic analysis. Earth. Eng. Struct. Dyn. 31:491–514. https://doi.org/10.1002/ege.141.
- [28] Güneş N (2020) Comparison of monotonic and cyclic pushover analyses for the near-collapse point on a mid-rise reinforced concrete framed building. Earthquakes and Structures 19:189–96. https://doi.org/10.12989/eas.2020.19.3.189.
- [29] Ibarra LF, Krawinkler H. (2005) Global Collapse of Frame Structures under Seismic Excitations. The John A. Blume Earthquake Engineering Center. Stanford University, CA.
- [30] Kırçıl MS, Polat Z (2006) Fragility analysis of mid-rise R/C frame buildings. Eng. Struct. 28:1335–45. https://doi.org/10.1016/j.engstruct.2006.01.004.
- [31] Baker JW (2015) Efficient analytical fragility function fitting using dynamic structural analysis. Earthq. Spectra 31:579–99. https://doi.org/10.1193/021113EQS025M.
- [32] Haselton CB, Baker JW, Liel AB, Deierlein GG (2011) Accounting for ground-motion spectral shape characteristics in structural collapse assessment through an adjustment for epsilon. J. Struct. Eng. 137:332–44. https://doi.org/10.1061/(ASCE)ST.1943-541X.0000103.
- [33] Lin T, Harmsen SC, Baker JW, Luco N (2013) Conditional spectrum computation incorporating multiple causal earthquakes and ground-motion prediction models. Bull. Seismol. Soc. Am. 103:1103–16. https://doi.org/10.1785/0120110293.
- [34] Lin T, Haselton CB, Baker JW (2013) Conditional spectrum-based ground motion selection. Part I: Hazard consistency for risk-based assessments. Earth. Eng. Struct. Dyn.42:1847–1865. https://doi.org/10.1002/eqe.2301.